Supplementary Material for

Structure of $NaFeSiO_4$, $NaFeSi_2O_6$, and $NaFeSi_3O_8$ glasses and glass-ceramics

Mostafa Ahmadzadeh,[a,c] Alex Scrimshire,[b] Lucy Mottram,[d] Martin C. Stennett,[d] Neil C. Hyatt,[d] Paul A. Bingham,[b] John S. McCloy[a,c,d,e,*]

[a]Materials Science and Engineering Program, Washington State University, Pullman, WA, 99164, USA

[b]Materials and Engineering Research Institute, Sheffield Hallam University, Sheffield S1 1WB, UK

[c]School of Mechanical and Materials Engineering, Washington State University, Pullman, WA, 99164, USA

[d]Department of Materials Science and Engineering, The University of Sheffield, Sheffield, S1 3JD, UK

[e]Institut de Physique du Globe de Paris, Équipe Géomatériaux, Paris, France

[*]Corresponding author, E-mail address: john.mccloy@wsu.edu

XRD Patterns

X-ray diffraction patterns for the as-quenched glasses (black) and heat-treated samples (red) are shown in Figure S1.

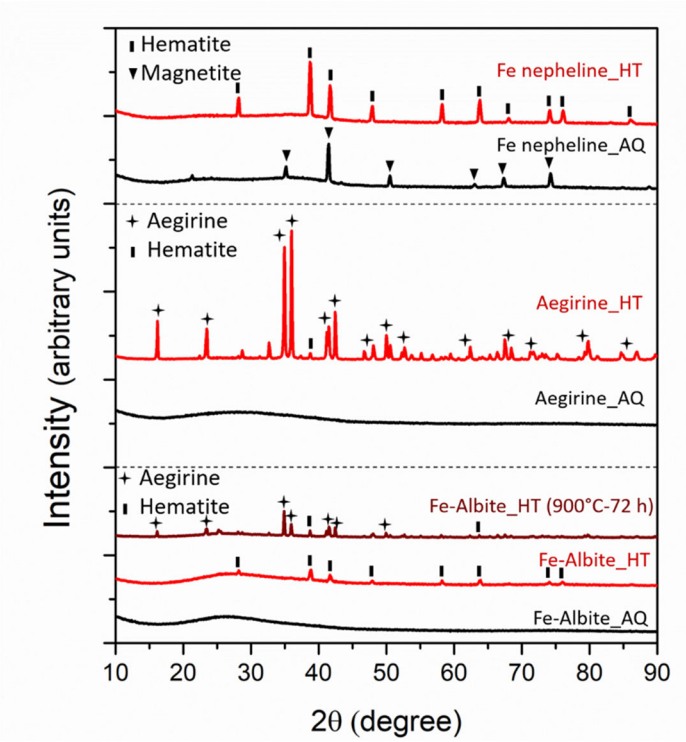

Figure S1. XRD patterns of as-quenched (AQ) and heat-treated (HT) $NaFeSiO_4$ (Fe-nepheline), $NaFeSi_2O_6$ (aegirine), and $NaFeSi_3O_8$ (Fe-albite).

Thermal Analysis

The DTA and TGA results of the three as-quenched glasses are presented in Figure S2. The Fe-nepheline glass, unlike the other two compositions, shows additional features (T_1, T_2, and T_3) in the range 400-800°C. The $NaFeSi_2O_6$ glass shows a sharp endothermic peak at 998°C (on-peak) which is due to the incongruent melting of aegirine with separation of hematite, as discussed in (Bowen et al., 1930). The other two glasses (Fe-nepheline and Fe-albite) do not show any sharp melting point since they remain mostly amorphous during heating and do not form a significant fraction of crystals with well-defined melting temperatures.

For all three studied compositions, the glasses gain less than 0.5% weight on heating to ~ 1100°C, which can be attributed to oxidation of Fe^{2+} to Fe^{3+} during heating (see Mössbauer section). The samples begin losing weight at temperatures >1100°C, which is most likely due to volatilization of Na at elevated temperatures.

The DTA thermograph of this sample shows two exothermic peaks (T_2 and T_3) in the range of 600-800°C. These peaks are attributed to the rejection of more iron from the glass, the presence of magnetite in the as-quenched material, and its transformations at elevated temperatures, including oxidation of magnetite to hematite which is suggested to begin at ~ 575°C and culminate at higher temperatures (Lepp, 1957).

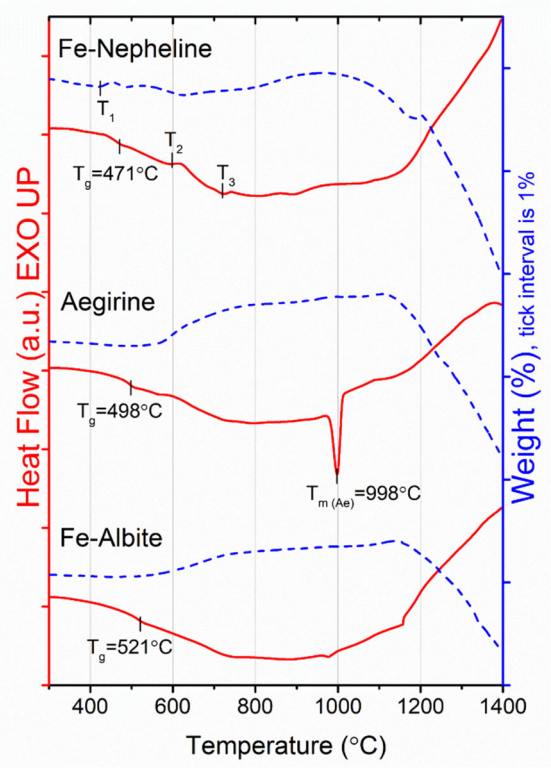

Figure S2. DTA (solid lines) and TGA (dash lines) thermographs for glasses with composition Fe-nepheline ($NaFeSiO_4$), aegirine ($NaFeSi_2O_6$), and Fe-albite ($NaFeSi_3O_8$), heated at 10°C min^{-1} under constant N_2 flow.

Magnetic Measurements

Such measurements can provide valuable insight into the iron-containing phases (Ahmadzadeh et al., 2017; Deshkar et al., 2017). The Fe-nepheline as-quenched sample reveals a clear saturating magnetic hysteresis loop with relatively high saturation magnetization, due to the presence of the ferrimagnetic magnetite phase within the amorphous glass. The aegirine and Fe-albite as-quenched samples, on the other hand, show a constant increase in the spontaneous magnetization with increasing field, and no magnetic saturation. This paramagnetic behavior is typical for iron-containing amorphous phases (Ahmadzadeh et al., 2017; Smirnov and Tarduno, 2003). Moreover, the as-quenched aegirine sample indicates slightly higher magnetization at a given field as it has a higher concentration of iron, the only present magnetic element, in the paramagnetic glass phase.

The magnetization curve of the heat-treated aegirine sample (900 °C - 24 h), shows contributions from both magnetically-ordered crystals and paramagnetic phase(s). As revealed by XRD results, this sample contains mostly aegirine crystals ($NaFeSi_2O_6$), with some hematite (Fe_2O_3) and residual glass. Aegirine is a low-temperature antiferromagnet with a Néel temperature (T_N) of ~8 K (Ballet et al., 1989; Baum et al., 1997) above which it becomes paramagnetic. However, pure hematite exhibits canted antiferromagnetism at room temperature with a small magnetization of ~ 0.4 Am^2/kg (Dunlop and Özdemir, 1977; Dunlop and Özdemir, 2007), and a relatively high coercive field. Therefore, the observed paramagnetism is from the aegirine phase at room temperature as well as the iron-containing residual glass, whereas the hysteresis behavior is likely due to hematite.

Mössbauer Spectroscopy

The fitted spectral parameters of room temperature Mössbauer spectra of Fe-nepheline, aegirine, and Fe-albite as-quenched samples as well as crystallized aegirine sample, are listed in Table S1. The values for Fe redox for wet chemical versus Mössbauer methods are listed in Table S2.

Table S1. Fitted Mössbauer parameters of the sodium iron silicate samples obtained from the corresponding spectra. CS is relative to α-Fe foil.

Sample	Signal	CS ± 0.02 (mm/s)	QS ± 0.02 (mm/s)	Hyperfine Splitting (T)	Area ± 2 (%)
Fe-nepheline_AQ	Doublet 1 (Fe^{3+})	0.24	0.86	-	76.4
	Sextet 1 (magnetite)	0.68	-	44.6	17.3
	Sextet 2 (magnetite)	0.28	-	48.5	6.3
Aegirine_AQ	Doublet 1 (Fe^{3+})	0.25	0.92	-	84.7
	Doublet 2 (Fe^{2+})	0.88	1.94	-	15.3
Fe-albite_AQ	Doublet 1 (Fe^{3+})	0.26	0.87	-	81.2
	Doublet 2 (Fe^{2+})	0.85	1.88	-	18.8
Aegirine-900°C-24h	Doublet 1 (Fe^{3+}, CN=4)	0.24	0.93	-	53.9
	Doublet 2 (Fe^{3+}, CN=6)	0.40	0.31	-	46.1

Table S2. Iron redox values obtained from Mössbauer spectroscopy (xVBF fits) and wet chemistry of as-quenched (AQ) aegirine and Fe-albite samples

			Aegirine_AQ	Fe-albite_AQ
$Fe^{3+}/\Sigma Fe$	Mössbauer Spectroscopy		0.847	0.812
	Wet chemistry	Average	0.833	0.815
		St. Dev.	0.002	0.004

Raman Spectroscopy

While the Raman spectroscopy discussion in this work is purely qualitative, both raw data as well as treated data are reported. Data treatment was carried out by correcting for temperature and excitation line per (Neuville and Mysen, 1996), then a linear baseline was subtracted, and all spectra were normalized to unit area for comparison. We refer the reader to Di Muro et al. (2009) for discussion of how different methods of treatment and baseline subtraction proposed in the

literature can affect the relative intensity and even the position of Raman bands in various iron silicate glasses.

Low frequency (LF~200-600 cm^{-1}), medium frequency (MF~600-800 cm^{-1}) and high frequency (HF~800-1200 cm^{-1}) envelopes are the three main bands in Raman spectra of most silicate glasses. The LF region in silicate networks is normally assigned to large-scale vibrations of rings of tetrahedra, whereas the HF envelope is conventionally attributed to stretching vibrations of metal-oxygen bonds in individual tetrahedra. The LF envelope, moreover, can potentially reveal some information regarding the inter-tetrahedral angle, the ring arrangement, $Si\text{-}O^0$ rocking motions, and Si-O-Si bending motions. The intermediate region (MF) is the weakest feature in such glasses and is controversially attributed to various vibrational modes (Di Genova et al., 2016; Di Muro et al., 2009; McMillan, 1984; Mysen et al., 1980; Neuville et al., 2014; Rossano and Mysen, 2012).

X-ray Absorption Spectroscopy

To calibrate the energy scale of the XANES data, the first peak in the first derivative of the reference Fe foil spectrum was set to 7112.00 eV (Bearden and Burr, 1967). Data calibration, normalization and background removal were performed on Athena, from the Demeter system (Ravel and Newville, 2005).

Processing and analysis of the Fe-K edge XANES pre-edge feature were performed using Microsoft Excel® software, as described in (Joseph et al., 2017). First, a spline function was fit to model the contribution of the edge step; this contribution was then subtracted to extract the pre-edge feature. The pre-edge feature was fitted with two Gaussian components (a third component was included dependent on the improvement in goodness of fit), and a total fit was calculated from the sum of these components. A linear least squares refinement was used to optimize the total fit

through adjustment of normalized component height, energy position, and full width at half height. The full width at half height was not constrained, to allow for best agreement between the total fit and the pre-edge feature. The centroid energy position was determined by taking the average centroid energy of the Gaussian components, weighted by intensity. This is a simplified form of the analysis method implemented by Wilke et al. (2001), which used pseudo-Voigt components with a fixed component shape of 50% Gaussian and 50% Lorentzian.

Related mineral systems

The naturally-occurring nepheline contains K in Na sites, (Na,K)$AlSiO_4$, and is the most abundant member of the feldspathoid group (Edgar, 1984). Nepheline has a hexagonal crystal structure with space group of $P6_3$. Jadeite is an important pyroxene mineral with monoclinic structure and space group $C2/c$, isostructural with aegirine (Nestola et al., 2007; Prewitt and Burnham, 1966). Low albite (completely ordered) is the sodium end member of plagioclase feldspar group which crystallizes in triclinic symmetry with space group of $C\bar{1}$ (Phillips et al., 1989). Crystallization of albite, however, is extremely difficult and slow in the Na_2O-Al_2O_3-SiO_2 system compared to other feldspars (Bowen and Schairer, 1938; MacKenzie, 1957; Tuttle and Bowen, 1950; Uhlmann et al., 1980; Zanotto and Cassar, 2017), though its hydrothermal synthesis has been reported (Martin, 1969). Figure S3 shows the structures of these three Al phases.

We can infer that Fe^{3+} can entirely substitute Al^{3+} in the sodium aluminosilicate phases in which aluminum is six-coordinated, i.e., form a full-range solid-solution (jadeite – aegirine). As verified by the Mössbauer spectrum for the crystallized aegirine sample (Figure 2d), iron is present as six-coordinated Fe^{3+} in the aegirine phase. However, in the sodium aluminosilicate structures in which Al^{3+} is tetrahedrally coordinated (nepheline and albite), iron can only partially substitute for aluminum.

While similar valence and ionic radii of Fe^{3+} and Al^{3+} lead to similar structural position of these two cations in silicate glasses, this analogy may not always hold true for silicate crystals (Mysen and Richet, 2005; Mysen and Virgo, 1978). As pointed out by Mysen (2005), in silicate crystals, four-coordinated Al^{3+} is common, whereas 4-coordinated Fe^{3+} is rare.

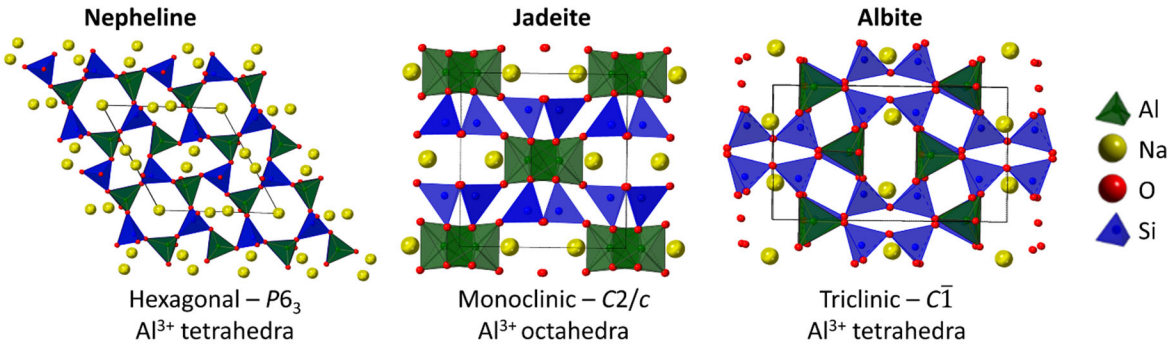

Figure S3. A representation of the crystal structures of nepheline – $NaAlSiO_4$ (Buerger et al., 1946), jadeite – $NaAlSi_2O_6$ (Prewitt and Burnham, 1966), and albite – $NaAlSi_3O_8$ (Winter et al., 1977). View is along c axis and the black boxes indicate a unit cell.

References

Ahmadzadeh, M., Marcial, J., and McCloy, J. (2017) Crystallization of iron-containing sodium aluminosilicate glasses in the $NaAlSiO_4$-$NaFeSiO_4$ join. Journal of Geophysical Research: Solid Earth, 122, 2504-2524.

Ballet, O., Coey, J.M.D., Fillion, G., Ghose, A., Hewat, A., and Regnard, J.R. (1989) Magnetic order in acmite; $NaFeSi_2O_6$. Physics and Chemistry of Minerals, 16, 672-677.

Baum, E., Treutmann, W., Lottermoser, W., and Amthauer, G. (1997) Magnetic properties of the clinopyroxenes aegirine and hedenbergite: a magnetic susceptibility study on single crystals. Physics and Chemistry of Minerals, 24, 294-300.

Bearden, J.A., and Burr, A.F. (1967) Reevaluation of X-Ray Atomic Energy Levels. Reviews of Modern Physics, 39, 125-142.

Bowen, N.L., and Schairer, J.F. (1938) Crystallization Equilibrium in Nepheline-Albite-Silica Mixtures with Fayalite. The Journal of Geology, 46, 397-411.

Bowen, N.L., Schairer, J.F., and Willems, H.W.V. (1930) The ternary system; Na_2SiO_3-Fe_2O_3-SiO_2. American Journal of Science, Series 5 Vol. 20, 405-455.

Buerger, M.J., Klein, G.E., and Hamburger, G. (1946) Structure of nepheline. Geological Society of America Bulletin, 57, 1182-1183.

Deshkar, A., Marcial, J., Southern, S.A., Kobera, L., Bryce, D.L., McCloy, J.S., and Goel, A. (2017) Understanding the structural origin of crystalline phase transformations in nepheline ($NaAlSiO_4$) based glass-ceramic. Journal of the American Ceramic Society, 100, 2859-2878.

Di Genova, D., Hess, K.U., Oryaëlle Chevrel, M., and Dingwell, D.B. (2016) Models for the estimation of Fe^{3+}/Fe_{tot} ratio in terrestrial and extraterrestrial alkali-and iron-rich silicate glasses using Raman spectroscopy. American Mineralogist, 101, 943-952.

Di Muro, A., Métrich, N., Mercier, M., Giordano, D., Massare, D., and Montagnac, G. (2009) Micro-Raman determination of iron redox state in dry natural glasses: Application to peralkaline rhyolites and basalts. Chemical Geology, 259, 78-88.

Dunlop, D.J., and Özdemir, Ö. (1977) Rock magnetism: fundamentals and frontiers. Cambridge University Press, New York.

Dunlop, D.J., and Özdemir, Ö. (2007) Magnetizations in rocks and minerals. In M. Kono, Ed. Geomagnetism, Treatise on Geophysics, 5, p. 278-331. Elsevier, Amsterdam.

Edgar, A.D. (1984) Chemistry, Occurrence and Paragenesis of Feldspathoids: A Review. In W.L. Brown, Ed. Feldspars and Feldspathoids: Structures, Properties and Occurrences, p. 501-532. Springer Netherlands, Dordrecht.

Joseph, K., Stennett, M.C., Hyatt, N.C., Asuvathraman, R., Dube, C.L., Gandy, A.S., Govindan Kutty, K.V., Jolley, K., Vasudeva Rao, P.R., and Smith, R. (2017) Iron phosphate glasses: Bulk properties and atomic scale structure. Journal of Nuclear Materials, 494, 342-353.

Lepp, H. (1957) Stages in the Oxidation of Magnetite. American Mineralogist, 42, 679-681.

MacKenzie, W.S. (1957) The crystalline modifications of $NaAlSi_3O_8$. American Journal of Science, 255, 481-516.

Martin, R.F. (1969) The hydrothermal synthesis of low albite. Contributions to Mineralogy and Petrology, 23, 323-339.

McMillan, P. (1984) Structural studies of silicate glasses and melts—applications and limitations of Raman spectroscopy. American Mineralogist, 69, 622-644.

Mysen, B.O., and Richet, P. (2005) Silicate glasses and melts: properties and structure. Elsevier, Amsterdam.

Mysen, B.O., and Virgo, D. (1978) Influence of pressure, temperature, and bulk composition on melt structures in the system $NaAlSi_2O_6$ -$NaFe^{3+}Si_2O_6$. American Journal of Science, 278, 1307-1322.

Mysen, B.O., Virgo, D., and Scarfe, C.M. (1980) Relations between the anionic structure and viscosity of silicate melts—a Raman spectroscopic study. American Mineralogist, 65, 690-710.

Nestola, F., Tribaudino, M., Boffa Ballaran, T., Liebske, C., and Bruno, M. (2007) The crystal structure of pyroxenes along the jadeite–hedenbergite and jadeite–aegirine joins. American Mineralogist, 92, 1492-1501.

Neuville, D.R., de Ligny, D., and Henderson, G.S. (2014) Advances in Raman spectroscopy applied to earth and material sciences. Reviews in Mineralogy and Geochemistry, 78, 509-541.

Neuville, D.R., and Mysen, B.O. (1996) Role of aluminium in the silicate network: In situ, high-temperature study of glasses and melts on the join SiO_2-$NaAlO_2$. Geochimica et Cosmochimica Acta, 60, 1727-1737.

Phillips, M.W., Ribbe, P.H., and Pinkerton, A.A. (1989) Structure of intermediate albite, $NaAlSi_3O_8$. Acta Crystallographica Section C, 45, 542-545.

Prewitt, C.T., and Burnham, C.W. (1966) The crystal structure of jadeite, $NaAlSi_2O_6$. American Mineralogist, 51, 956-975.

Ravel, B., and Newville, M. (2005) ATHENA, ARTEMIS, HEPHAESTUS: data analysis for X-ray absorption spectroscopy using IFEFFIT. Journal of Synchrotron Radiation, 12, 537-541.

Rossano, S., and Mysen, B. (2012) Raman spectroscopy of silicate glasses and melts in geological systems. In J. Dubessy, M.-C. Caumon, and F. Rull, Eds. Raman spectroscopy applied to Earth sciences and cultural heritage, 12. Mineralogical Society of Great Britain and Ireland.

Smirnov, A.V., and Tarduno, J.A. (2003) Magnetic hysteresis monitoring of Cretaceous submarine basaltic glass during Thellier paleointensity experiments: evidence for alteration and attendant low field bias. Earth and Planetary Science Letters, 206, 571-585.

Tuttle, O.F., and Bowen, N.L. (1950) High-Temperature Albite and Contiguous Feldspars. The Journal of Geology, 58, 572-583.

Uhlmann, D.R., Yinnon, H., and Cranmer, D. (1980) Crystallization Behavior of Albite. Lunar and Planetary Science Conference, p. 1178-1180.

Wilke, M., Farges, F.o., Petit, P.-E., Brown, G.E., Jr., and Martin, F.o. (2001) Oxidation state and coordination of Fe in minerals: An Fe K-XANES spectroscopic study. American Mineralogist, 86, 714-730.

Winter, J.K., Ghose, S., and Okamura, F.P. (1977) A high-temperature study of the thermal expansion and the anisotropy of the sodium atom in low albite. American Mineralogist, 62, 921-931.

Zanotto, E.D., and Cassar, D.R. (2017) The microscopic origin of the extreme glass-forming ability of Albite and B_2O_3. Scientific Reports, 7, 43022.